Delft University of Technology

Less is more

Optimisation of variable catalyst loading in CO$_2$ electroreduction

Blake, J. W.; Haverkort, J. W.; Padding, J. T.

Important note
To cite this publication, please use the final published version (if applicable).
Please check the document version above.

Contents lists available at ScienceDirect

Electrochimica Acta

journal homepage: www.journals.elsevier.com/electrochimica-acta

Less is more: Optimisation of variable catalyst loading in CO_2 electroreduction

J.W. Blake *, J.W. Haverkort, J.T. Padding

Department of Process and Energy, Delft University of Technology, Leeghwaterstraat 39, 2628 CB Delft, The Netherlands

ABSTRACT

The electrochemical conversion of CO_2 is a promising method of carbon-neutral chemical production. However, commercial realisation in aqueous electrolytes is challenging, due to competition with the hydrogen evolution reaction (HER), and the propensity for CO_2 to participate in the carbonate equilibrium reactions. These two phenomena are linked through OH^- ions, as both the by-product of the catalytic reactions and the culprit behind the parasitic carbonate reactions. By reducing the local catalyst loading where the CO_2 concentration is low, the HER is decreased more than the reactions that are dependent on CO_2 as a reactant. Therefore, it is possible to improve reaction selectivity and reactant utilisation while reducing the capital cost of catalyst. We demonstrate this theory through an analytical solution of a 1D flow electrolyser model. We extend this to a comprehensive model of a contemporary gas-diffusion electrode (GDE) setup. We find that the operation costs are dominated by the electrolyser power consumption and, to a lesser degree, the cost of CO_2 and its recovery at the anode. We numerically obtain the catalyst loading profiles that maximise operating profit. The optimisation process reveals that profits are maximised for high gas flow rates, and consequently, low single pass conversions, where the CO_2 concentration is as high as possible. However, when lower gas flow rates are used for practical reasons, variable catalyst loadings are shown to lead to significant operational improvements, especially in the production of higher C products that require a greater number of electrons transferred. The model is made freely available in MATLAB and its use is encouraged in determining the applicability of variable catalyst loading to future experimental setups.

1. Introduction

As improvements in the fundaments of CO_2 electroreduction (CO_2ER) shift the field closer to industrial readiness, the focus on groundbreaking new insights naturally gives way to a focus on delicate optimisation and pragmatism. Catalysts are expected to be tested in less forgiving conditions [1–4], cells are expected to be stable even in the presence of feedstock impurities [5,6], electrolysers are expected to be scalable to industrial sizes [7–9], and techno-economic assessments (TEAs) are taking centre stage for their insights on realistic limitations [10]. Even at the laboratory scale, CO_2 electrolysers can exhibit non-uniformity. Simonson et al. showed a significant change in product selectivity over the reactor path in a gas-diffusion electrode (GDE) [11], and computational models have investigated these effects in limiting cases [8,12]. These non-uniformities are potentially due to a number of changes to the environments of the electrolyte, the catalyst layer, and the diffusion media, as well as due to the inherent reduction in reactant availability in high single-pass conversion setups. Circumventing these issues usually comes at some great cost; reductions

in conductivity, reactant utilisation, faradaic efficiency (FE), mass transport, and current density are seldom greater detriments to cell performance than the non-uniformities.

Noting the insights of Kulikovsky into polymer electrolyte fuel cell (PEFC) catalyst optimisation [13,14], we propose that CO_2 electroreduction can benefit greatly from catalyst loading optimisation. While Kulikovsky's work elegantly homogenises local current along the oxygen channel of a PEFC [15], the CO_2ER is complicated by the bicarbonate buffer system, a variable product spectrum, and an often unwanted hydrogen evolution (HER) side reaction. These effects are susceptible to modification through changes in local catalyst loading, and we propose a surprisingly efficacious model and method of catalyst loading optimisation for CO_2ER.

Many literature studies focus on a single aspect of a system, and often the improvement of such an aspect comes at the great cost of another aspect outside of the scope of that study. This is often the case in CO_2ER, with studies that optimise FE, conversion, cell potential, or reactant utilisation, but only by sacrificing their complementary

---

* Corresponding author.
E-mail address: J.W.Blake@tudelft.nl (J.W. Blake).

aspects. For instance, a high single pass conversion necessarily involves reactant depletion, which will lead to a drop in FE. One must consider whether the improvement in one aspect is worth the trade-off in another. This is the core of the idea behind variable catalyst loading, as local reducing the amount of available catalyst will clearly reduce the ability of the system to convert reactant in that region, but in return it can produce a more favourable environment in terms of selectivity and reactant utilisation. There are a large number of interacting aspects relevant when considering a GDE system, so we first lay out the basic idea before continuing.

2. 1D flow cell model

In the case of a well-mixed, flow-driven electrochemical reactor with a flow channel of length L, we can approximately model the system with a 1D first-order reaction-advection equation on the interval [0,L],

$$U\frac{\partial c}{\partial x} + kc = 0, \qquad c(0) = c_0, \tag{1}$$

where U is flow velocity, c is reactant concentration, c_0 is initial reactant concentration, and k [s^{-1}] is the (effective, volumetric, first order) reaction rate. To transform this into an equation for CO_2ER we must make some assumptions. We first note that the reaction usually takes place in neutral or alkaline media, so we will henceforth assume only the alkaline pathways of reactions. We take c to be the concentration of CO_2 and assume reactions of the form:
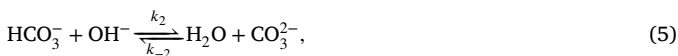
$$CO_2 + ne^- \xrightarrow{k} nOH^- + P, \tag{2}$$

where n is the number of electrons transferred per CO_2 molecule, k is the first order reaction rate and P denotes the products and, with a negative sign, other reactants like water. While only considering first order reactions may appear to strongly limit the generality, generally n is an integer multiple of two for each product pathway. Therefore, we can safely treat reactions to C_{2+} products that involve two CO_2 molecules by halving the reaction terms to preserve the form in (2). Furthermore, we note that there is also a parallel hydrogen evolution reaction in the form of

$$2H_2O + 2e^- \xrightarrow{k_{H_2}} 2OH^- + H_2, \tag{3}$$

where it is assumed that the concentration of the H_2O reactant remains constant and uniform and k_{H_2} [mol m^{-3} s^{-1}] is the zeroth order reaction rate.

Due to the production of OH^- in (2) and (3), the local environment will be in the neutral to alkaline pH range. The buffer reactions,

$$CO_2 + OH^- \underset{k_{-1}}{\overset{k_1}{\rightleftharpoons}} HCO_3^-, \tag{4}$$

$$HCO_3^- + OH^- \underset{k_{-2}}{\overset{k_2}{\rightleftharpoons}} H_2O + CO_3^{2-}, \tag{5}$$

convert CO_2 to bicarbonate (HCO_3^-) and carbonate (CO_3^{2-}) in an attempt to reduce the pH. The forward and backward reaction rate constants $k_{1,-1}$ and $k_{2,-2}$ pertain to conversion to HCO_3^- and CO_3^{2-}, respectively. The rate constants k_2 and k_{-2} are relatively large, so it is almost always the case that HCO_3^-, OH^-, and CO_3^{2-} are in equilibrium, but k_1 and k_{-1} are much smaller, so it is often the case that CO_2 is out of equilibrium with OH^- and HCO_3^-. Moore et al. exploited this disparity to develop simplified models for the buffer system at varying pH ranges [16].

2.1. Catalyst loading

Catalyst loading is usually expressed in units of mg cm^{-2}, but here the focus is on the relative catalyst loading. We will exclusively use a dimensionless catalyst loading $\theta \in [0, 1]$, where $\theta = 1$ corresponds to the maximal catalyst loading at the inlet of the reactor. We assume that the electrochemical reaction kinetics are linear in catalyst loading

and express the (effective, volumetric) electrochemical reaction rates [mol/m^3/s] as

$$R_{CO_2} = \theta ck, \tag{6}$$

$$R_{H_2} = \theta k_{H_2} = \frac{\theta c_0 k}{q}. \tag{7}$$

Here, $q \equiv c_0 k/k_{H_2}$ is the ratio between the CO_2 and H_2 reaction rate constants at the inlet CO_2 concentration, c_0. As Kulikovsky notes, this assumption of linear scaling with θ is valid for an ideally constructed porous catalyst medium [14]. We herein assume that the medium is ideal, but not that in a realistic medium it is impossible to vary catalyst loading without also varying the porous structure, affecting mass transfer, and potentially reducing the effective available catalyst surface area per unit catalyst through pore blockage or overlap. Nonetheless, if the maximal catalyst loading θ_0 is small compared to the capacity for catalyst in the porous matrix, the relationship with exchange current density will explicitly be linear with θ, but reaction rate will still implicitly depend nonlinearly on θ in Eq. (6) through its dependence on c, which is a function of θ. Larrazábal et al. noted that if the OH^- produced in (2) is to immediately and fully react with CO_2 through (4) and (5), then maximum conversion efficiency is governed by the stoichiometry of the product [4]. That is to say, one mole of CO_2 reactant participating in an electrochemical reaction with n moles of electrons transferred will subsequently cause $\frac{n}{2}$ moles of CO_2 to react with the n moles of electrochemically produced OH^-, limiting conversion efficiency to a maximum of $\frac{2}{n+2}$, with lower values to be expected once the HER is included. Moore et al. cleanly showed that collapsing (4) and (5) into a single irreversible reaction is valid at high pH, and detailed a simplified model similar to our approach [16]. We still wish to include the effect of OH^- production from the HER (3) on the CO_2ER reaction rate. Therefore, we rewrite (1) for the evolution of the CO_2 concentration c to

$$U\frac{\partial c}{\partial x} + \underbrace{\theta ck}_{} + \underbrace{\frac{n}{2}\theta ck}_{} + \underbrace{\frac{\theta c_0 k}{q}}_{} = 0. \tag{8}$$
$$\text{advection} \quad \text{reduction} \quad OH^- \text{ from (2)} \quad OH^- \text{ from (3)}$$

Here, the $\frac{n}{2}$ term comes from the assumption that each CO_2 electrochemically converted will produce nOH^-, half of which will react with CO_2 via (4) and half via (5), consuming a total of $\frac{n}{2}$ additional CO_2 molecules. Nondimensionalising gives

$$\frac{\partial \bar{c}}{\partial \bar{x}} + Da\,\theta\left(\left(1 + \frac{n}{2}\right)\bar{c} + \frac{1}{q}\right) = 0, \qquad \bar{c}(0) = 1 \tag{9}$$

where $\bar{c} \equiv \frac{c}{c_0}$, $\bar{x} \equiv \frac{x}{L}$, and $Da \equiv \frac{kL}{U}$. Da is the initial Damköhler number, representing the ratio between the reaction rate at the inlet (i.e. the reaction rate if the entire channel would have uniform catalyst loading equal to that at the inlet) and convective mass transport. In Ref. [17] an extension of (8) is discussed, including the effect of a laminar flow profile and mass transfer resistances between the flow channel and the catalyst layer. The latter can be included by adding to the inverse of k, in the second and third term, the inverse of a mass transfer coefficient k^t.

The two dimensionless metrics of primary interest are the faradaic efficiency or selectivity, S, and the inlet-normalised yield, Y,

$$S \equiv \frac{\int_0^L \theta nkc\,dx}{\int_0^L \theta(nkc + 2k_{H_2})\,dx} \equiv \frac{\int_0^1 \theta nq\bar{c}\,d\bar{x}}{\int_0^1 \theta(nq\bar{c} + 2)\,d\bar{x}} \tag{10}$$

$$Y = \frac{1}{Uc_0}\int_0^L \theta kc\,dx = \int_0^1 Da\theta\bar{c}\,d\bar{x}. \tag{11}$$

In the second expression of (10) the rate constants k and k_{H_2} are assumed to be constant. A figure of note is the cumulative catalyst loading, $\Theta(\bar{x})$, defined by

$$\Theta(\bar{x}) \equiv \int_0^{\bar{x}} \theta(\xi)d\xi, \quad \text{or} \quad \Theta \equiv \int_0^1 \theta(\xi)d\xi. \tag{12}$$

The yield, Y, is not to be confused with normalised CO_2 conversion X,

$$X = \frac{1}{Uc_0} \int_0^L \theta k \left(\left(1 + \frac{n}{2}\right) c + \frac{c_0}{q} \right) dx = Da \int_0^1 \theta \left(\left(1 + \frac{n}{2}\right) \bar{c} + \frac{1}{q} \right) d\bar{x}, \tag{13}$$

which includes the unwanted buffer reactions. The astute observer may note that by the fundamental theorem of calculus and (9), it holds that $X = 1 - \bar{c}(1)$.

The solution to (9) for $\theta \equiv 1$ (uniform loading) is

$$\bar{c} = \frac{\left(1 + \left(1 + \frac{n}{2}\right) q\right) e^{-\left(1 + \frac{n}{2}\right) Da \ \bar{x}} - 1}{\left(1 + \frac{n}{2}\right) q} \xrightarrow{q \to \infty} e^{-\left(1 + \frac{n}{2}\right) Da \ \bar{x}} \xrightarrow{n=2} e^{-2Da \ \bar{x}}. \tag{14}$$

While in the limit of no side-reactions, $q \to \infty$, the concentration stays non-negative, this is not guaranteed for general q. Therefore (14) only holds when it gives a positive value and should be replaced by 0 for negative outcomes. Equivalently an additional requirement of $X \leq 1$ can be made to ensure that we remain within the domain of validity of the approximation.

As an example case we consider $n = 2$, corresponding to CO_2 reduction to CO. For $\theta \equiv 1$

$$\bar{c} = \frac{1}{2q}((1 + 2q)e^{-2Da \ \bar{x}} - 1). \tag{15}$$

For a linearly decreasing loading, $\theta = 1 - A\bar{x}$, the solution is given by

$$\bar{c} = \frac{1}{2q} \left((1 + 2q) e^{-Da\bar{x}(2 - A\bar{x})} - 1 \right), \tag{16}$$

where $A \in [0, 1]$. A full description and derivation of these solutions, and solutions of additional cases can be found in the Supplementary Information, Section SI 1.

We note again that the Damköhler number referred to in (9) is specifically for the catalyst loading at the entrance of the channel: the final Damköhler number will depend on the total catalyst loading as ΘDa, with more explanation found in SI 1.4.

2.2. Results

To determine the effectiveness of a proposed catalyst loading profile we must decide on an effectiveness metric. It is clear from (10) that maximising the FE is equivalent to maximising $\bar{c}$, which requires minimising θ (see (S4) or (S15)). However, maximising yield, Y, defined in (12), will likely require maximising θ. We thus propose a metric $\mathcal{E} = $ YS, the product of yield and FE, which combines how much product is made with how efficiently it was attained. This is a necessarily simplistic metric, but a much more in-depth metric is discussed in Section 3.2.

Fig. 1 shows the solution of (15) for a homogeneous catalyst loading and $n = 2$. As the ratio q between CO_2 and H_2 reaction rate constants increases, the CO_2 concentration increases due to a decrease in parasitic buffer reactions.

Figs. 2 (a) and (b) show the solution of (16) for a linearly decreasing catalyst loading and $n = 2$ without homogeneous reactions ($n = 0$ and $q \to \infty$), similar to Kulikovsky [15]. The solutions for this case are discussed in the SI. A maximum effectiveness of 1 can be obtained in this case, for high q and Da. At lower q a maximum arises at intermediate Da.

Figs. 2(c) and (d) include the effect of the homogeneous reactions. It may be noted that the maximum effectiveness does not surpass 0.5. This is due to the maximum yield of 0.5, with OH^- produced by CO_2ER consuming at least half of the CO_2 through the buffer reactions. Otherwise, the results are qualitatively quite similar to those in the absence of buffer reactions.
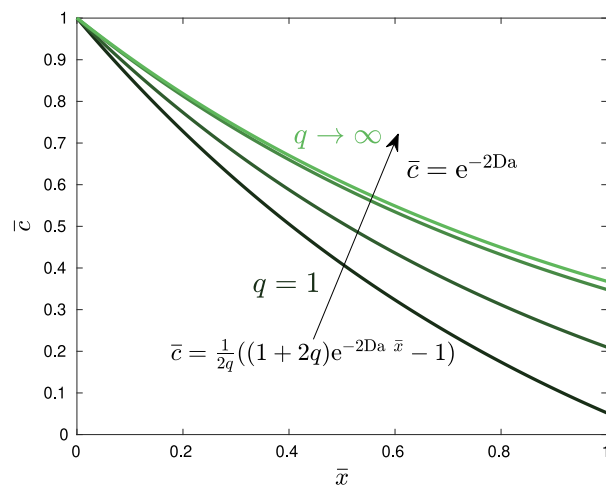

Fig. 1. The dependency of the normalised concentration $\bar{c}$ in (15) on the ratio q of CO_2 and H_2 reaction rates for an $n = 2$ electron reaction with uniform catalyst loading. As q increases, the solution collapses onto the stoichiometry limited solution proposed in Ref. [4].

No direct general improvement in the effectiveness, $\mathcal{E}$, can be obtained by reducing the catalyst loading, but for a fixed Da a decreased catalyst loading can increase the effectiveness. An equal effectiveness can always be obtained using a flat catalyst loading, by choosing the optimal value of Da, and the derivation of optimal values in SI 1.4 shows that the reverse is possible too. Any local optimum achieved using a flat catalyst loading can be matched by reducing catalyst loading in a system with a higher fixed Da. Note that, unless q is very large, this optimal Da is typically around or slightly above 1. The reason is that at low Da the concentration varies little and the S is highest. However, at high Da, the conversion and yield are much higher, giving an optimum at intermediate values.

In SI 1.4 we also analytically determine the location of the optimal value of the product $Da\Theta$ in terms of q. The solution for the case without buffer reactions can be approximated with a maximum relative error of 11% by

$$(\Theta Da)_{opt} \approx 1 + \ln \left(\frac{1.2923q}{\ln(1 + q)} \right) \tag{17}$$

which is exact in the limit $q \to 0$. However, in this limit $\mathcal{E} \to 0$ and for $q \gg 1$ a better approximation is the simple approximation $(\Theta Da)_{opt} \approx \ln(q)$. For the cases with homogeneous reactions, similar results can be found with approximations accurate to about 7% for low to moderately high $0 \leq q \lesssim 10^3$, and exact in the limit of low q,

$$(\Theta Da)_{opt} \approx \frac{2}{3} W(q) \approx \frac{4}{3} \frac{1 + q/2}{1 + q} \ln \left(\frac{q}{\ln(1 + q)} \right), \tag{18}$$

and an accurate simple approximation for $q \gtrsim 10^2$ with $(\Theta Da)_{opt} \approx \frac{1}{2} \ln \left(\frac{2q}{3} \right)$ Using (17) and (18) the optimal flow velocity can be chosen based on the channel length and reaction rates.

As shown, this approach can reap some benefits in a simple flow reactor. In the most realistic case, Fig. 2(d), it is seen that the same effectiveness can be attained with reduced catalyst loading at a higher Damköhler number, representing a reduction in both capital cost of catalyst and operational pumping costs. We extend the model to a system more suited for industrial CO_2ER to determine the improvements that can be made in the more extreme conditions found in a GDE electrolyser.

3. GDE model

To overcome the prohibitively low solubility and diffusivity of CO_2 in aqueous electrolytes, GDEs are commonly used to supply gaseous
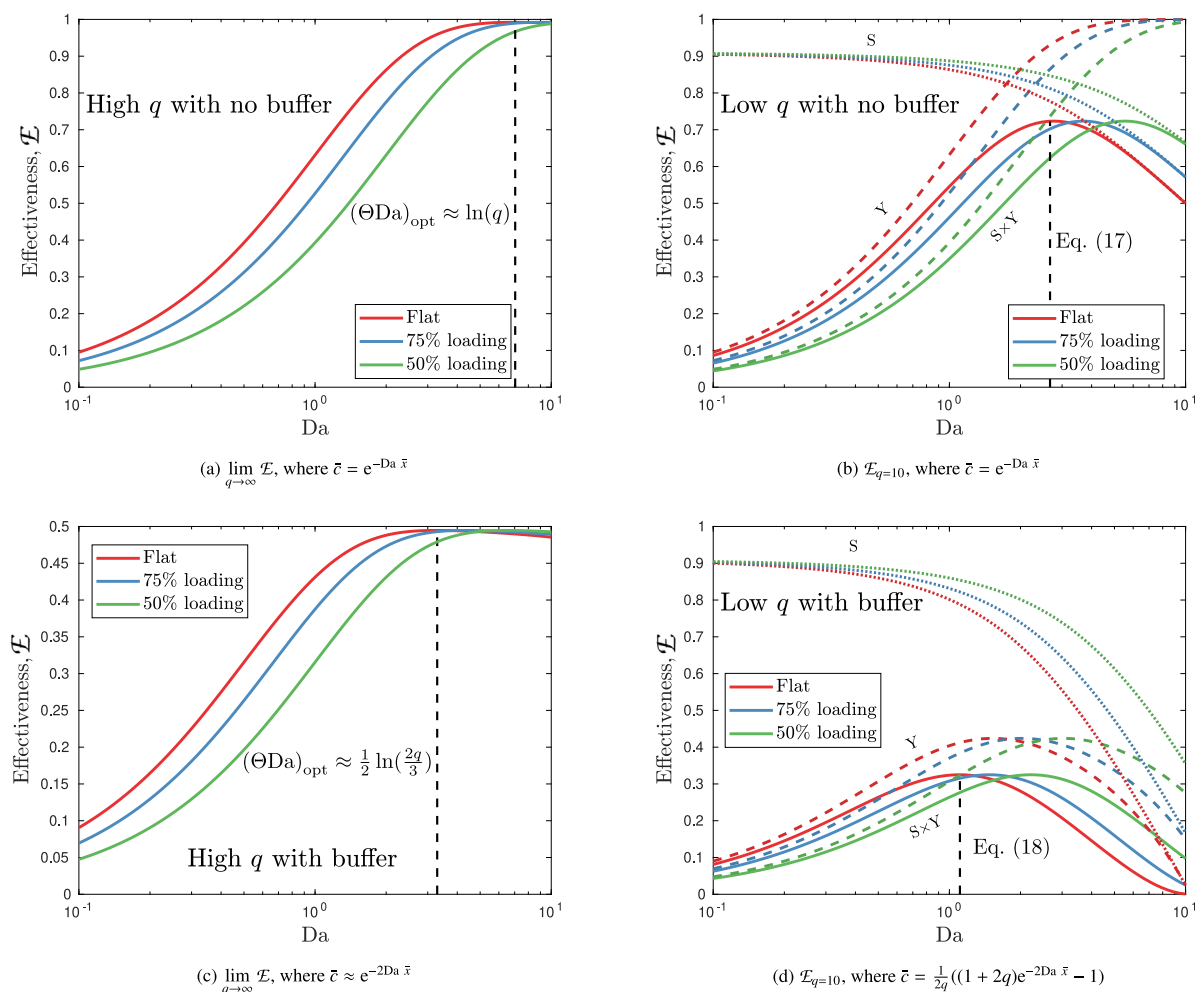
Fig. 2. A comparison of effectiveness, $\mathcal{E} = YS$, for linearly decreasing catalyst loadings for the system without homogeneous reactions with high $q \to \infty$, 2(a), and relatively low $q = 10$, 2(b) and for the system with approximate homogeneous reactions with high $q \to \infty$, 2(c), and relatively low $q \to \infty$, 2(d), for an $n = 2$ electron reaction. Red, blue and green colours indicate $A = 0$, 0.5 and 1, corresponding to 100%, 75% and 50% cumulative catalyst loading, respectively. For the low $q = 10$ case, dotted lines show the respective selectivities, S, and dashed lines show the respective yields, Y. In 2(c) and 2(d) the CO_2 buffer reactions lower the maximum yield and hence maximum effectiveness to 0.5, although 2(c) still exhibits behaviour similar to 2(a). In the most realistic system, 2(d), effectiveness remains low throughout due to reaction with OH^- sourced from both the CO_2ER (2) and HER (3).

CO_2 as close to the reaction sites as possible, minimising diffusive path length. This means that reactant depletion occurs in a parallel gas channel, and we must consider the transport of this depleted reactant to the reaction site. Furthermore, employed electrolytes are commonly optimised for high conductivity (e.g. KOH) or CO_2 saturation and buffer capacity ($KHCO_3$), both of which can affect the local buffer reaction and break the stoichiometric limit of Fig. 1. The diagram in Fig. 3 shows the normal operation of such an electrolyser, in which gas phase CO_2 is transported from the gas channel through the diffusion medium to dissolve in the electrolyte in the catalyst layer (CL), where it reacts at the catalyst sites. This, along with the undesired HER, produces OH^- ions that then aggressively react with the remaining aqueous CO_2 molecules, forming HCO_3^- and then CO_3^{2-}. Depending on the choice of electrolyte, there are additional sources, or sinks, of CO_2 and OH^- from the electrolyte. If a high pH electrolyte such as KOH is used, the concentration of OH^- in the bulk electrolyte will exceed that in the CL and act as a source, but a lower pH electrolyte can act as a OH^- sink, and in the case of CO_2 saturated $KHCO_3$, even act as a source of reactant CO_2. The extremely high CO_2 mass transfer rate offered by the GDE means that within the CL the CO_2 concentration is often out of equilibrium with the OH^- concentration, although equilibrium is still assumed in (5) with CO_3^{2-}. Thus, to model the behaviour upon reducing catalyst loading, as illustrated in Fig. 4, we are also required to independently consider the balance of OH^- and gaseous CO_2.

The effective utilisation of catalyst in GDEs has been investigated in the context of exchange current density. Sun et al. noted that reports of exchange current densities vary wildly between practical GDEs and rotating-disc electrodes (RDEs), and endeavoured to construct extremely well-defined mass transport conditions with a thin catalyst layer RDE setup and varying catalyst mass loadings while holding catalyst wt% constant [18]. Across each wt% bracket, they found results consistent with linear correlation coefficients of 0.99, 0.97, and 0.92 for 0.02wt%, 0.1w%, and 0.5wt% respectively, and conclude that erroneously low reports of exchange current density are due to failure to correct for mass transport limitations. We posit that the assumption of a linear explicit dependence of reaction rate on θ remains valid in this model so long as the CL structure remains unchanged for each value of θ, as mass transport limitations are independently included. We concede that a large increase in catalyst loading could still affect the porous structure, but note that we only consider a selective reduction in catalyst loading, so the porous structure should remain largely unchanged, provided θ_0 is not already extremely large.

3.1. Theory

First, we note that the system is governed by the spatial development of three correlated species: $OH^-_{(aq)}$, $CO_{2(aq)}$, and $CO_{2(g)}$. We also
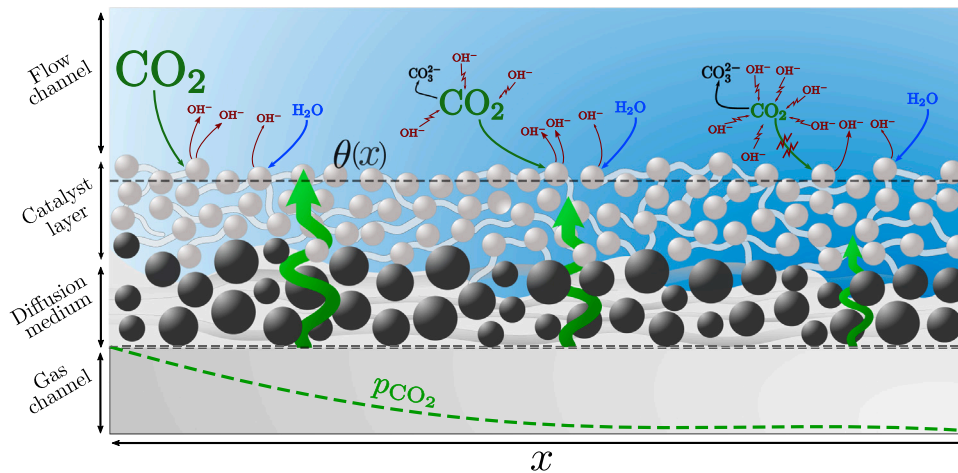
Fig. 3. A typical GDE flow electrolyser with uniform catalyst loading. High OH^- production leads to high parasitic consumption of CO_2 through buffer reactions and severe depletion of both aqueous and gaseous reactants.
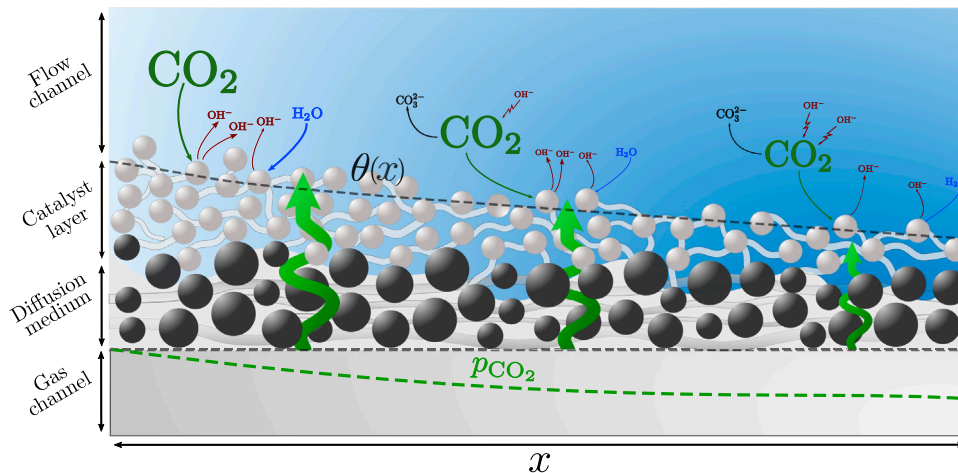

Fig. 4. A GDE flow electrolyser with progressively decreasing catalyst loading. Lower reduction reaction rates lead to improved CO_2 utilisation and reaction selectivity due to lower buffer reaction rates, at the cost of lower single-pass conversion.

note that there is little variation in the flow-perpendicular in-plane direction, and the characteristic in-plane length scales are far greater than the through-plane length scales, so it is pertinent to reduce the system from 2D to a 1D system with additional relations capturing the through-plane effects. The gas phase is flow-driven and is modelled by a simple ODE. It practically always has a sufficient Péclet number to neglect diffusion in the flow direction, so gas concentration c_g is modelled by

$$-\text{UL}_{\text{GC}} \frac{\partial c_g}{\partial x} = k^t_{\text{GC}}(\mathcal{H}^{cc} c_g - c), \qquad (19)$$

with c the average concentration $[CO_2]_{(aq)}$ in the catalyst layer. U is the average flow velocity [m/s] in the gas channel of width L_{GC} and k^t_{GC} is the mass transfer coefficient [m/s] between the gas channel (GC) and catalyst layer (CL). Here, t stands for transport, to make the distinction with reaction rate constants that lack this superscript. $\mathcal{H}^{cc}$ is the dimensionless concentration-to-concentration Henry's constant, which for an ideal gas can be related to the more common partial pressure-to-concentration Henry's constant through $\mathcal{H}^{cc} = \mathcal{H}RT$, where R is the molar gas constant and T is temperature. Introducing an aqueous-equivalent concentration $\mathbb{c} \equiv \mathcal{H}^{cc} c_g$ gives

$$-\frac{\text{UL}_{\text{GC}}}{\mathcal{H}^{cc}} \frac{\partial \mathbb{c}}{\partial x} = k^t_{\text{GC}}(\mathbb{c} - c), \qquad (20)$$

We will write the equilibrium concentration in the aqueous phase at the partial pressure of the gas inlet $c_0 = \mathcal{H} p_{CO_2,0} = \mathcal{H}^{cc} c_{g,0}$. Using this,

(19) can be nondimensionalised as

$$-\frac{\text{Da}_{\text{GC}}}{\mathcal{H}^{cc}} \frac{\partial \bar{\mathbb{c}}}{\partial \bar{x}} = \bar{\mathbb{c}} - \bar{c}, \qquad (21)$$

where $\bar{x} \equiv \frac{x}{\text{L}}$, $\bar{\mathbb{c}} \equiv \frac{\mathbb{c}}{c_0}$, $\bar{c} \equiv \frac{c}{c_0}$. $\text{Da}_{\text{GC}} \equiv \frac{\text{UL}_{\text{GC}}}{k^t_{\text{GC}}\text{L}}$ can be interpreted as a gas channel Damköhler number. Within the catalyst layer there is negligible flow, and the effect of diffusion parallel to the flow channel is minuscule compared to the through-plane interaction with the electrolyte and gas channels. Therefore, we let the spatial variation of the aqueous species along the CL be entirely determined by their local reaction rates and interactions with neighbouring channels. If we again restrict ourselves to the case of $n = 2$, this leads to the following local species balances for $CO_{2(aq)}$ and $OH^-_{(aq)}$ respectively,

$$\underbrace{k^t_{\text{GC}}(\mathbb{c} - c)}_{\text{transfer from gas channel}} + \underbrace{k^t_{CO_2}(c^{\text{B}} - c)}_{\text{transfer from electrolyte channel}} = \underbrace{\text{L}_{\text{CL}}\epsilon kc}_{CO_2\text{ER reaction}} + \underbrace{\text{L}_{\text{CL}}\epsilon k_r c_{OH^-} c}_{\text{homogeneous reaction}}, \qquad (22)$$

$$\underbrace{k^t_{OH^-}(c^{\text{B}}_{OH^-} - c_{OH^-})}_{\text{transfer from electrolyte channel}} + \underbrace{2\text{L}_{\text{CL}}\epsilon kc}_{CO_2\text{ER reaction}} + \underbrace{2\text{L}_{\text{CL}}\epsilon k_{H_2}}_{H_2\text{ evolution}} = \underbrace{2\text{L}_{\text{CL}}\epsilon k_r c_{OH^-} c}_{\text{homogeneous reaction}}, \qquad (23)$$

with c_{OH^-} the concentration $[OH^-]_{(aq)}$ at the catalyst layer (see Fig. 5). The constants we will use in our model calculations are listed in Table 1. Here, $k^t_{CO_2}$ refers to the mass transfer coefficients [m/s] of CO_2
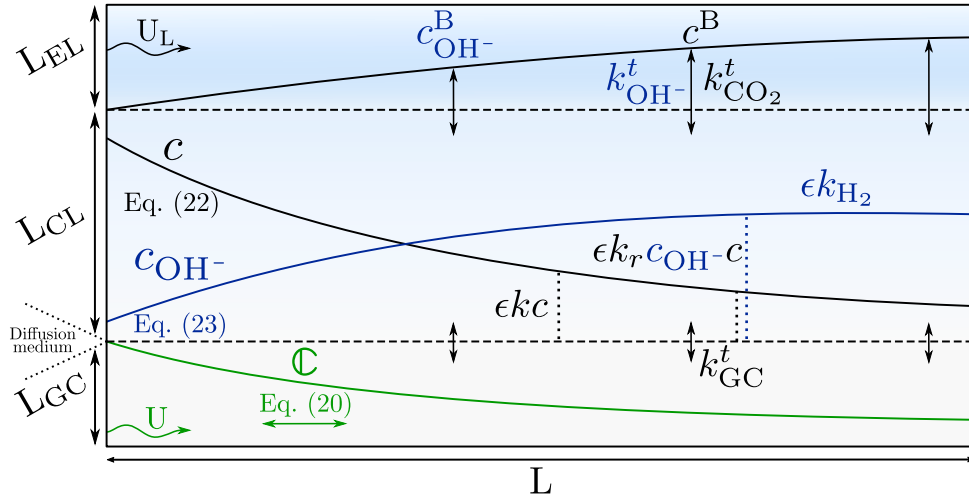
Fig. 5. Diagram of the numerical system (not to scale). Explicit variation in the flow-wise direction only occurs in the development of $\mathbb{c}$, through (20), and in the development of the boundary layer dependent mass transfer coefficients, $k_{OH^-}^t$ and $k_{CO_2}^t$. The concentrations c and c_{OH^-}, governed by (22) and (23) respectively, depend on these parallel streams, as well as each other and θ.

from the bulk of the electrolyte channel to the CL. The bulk concentrations in the electrolyte channel are given by c^B and $c_{OH^-}^B$, with the B superscript referring to bulk concentration. In each case, mass transfer from neighbouring channels is equated to volumetric sources/sinks due to reactions, averaged across the CL. In (22), CO_2 is being supplied by or lost to the electrolyte channel, depending on the value of c^B relative to c, and similarly for $c_{OH^-}^B$ and c_{OH^-} in (23). We note that we will likely see $c_{OH^-}^B > c_{OH^-}$ and $c > c^B$ in high pH electrolytes, like KOH, with the reverse being true for neutral pH electrolytes, like $KHCO_3$. The CO_2 then reacts through the thickness of the CL, L_{CL}, both electrochemically and with OH^-. A similar balance is in (23), but with no gas channel transfer. The same homogeneous reaction sink of $CO_{2(aq)}$ on the right-hand side of (22) appears for $OH^-_{(aq)}$ on the right-hand side of (23). It is doubled due to the second OH^- ion consumed in converting HCO_3^- to CO_3^{2-} in (5). The CO_2ER reaction sink $CO_{2(aq)}$ appears doubled and as a source of $OH^-_{(aq)}$, because we consider $n = 2$ in (2). Finally, also in the HER source of $OH^-_{(aq)}$ a factor 2 appears, because through (3) two $OH^-_{(aq)}$ ions are produced for each H_2.

In non-dimensionalising (22) and (23) we elect to divide by a characteristic value $\epsilon L_{CL} k_r c_0 c_{OH^-}^B$ of the homogeneous term giving

$$\underbrace{\bar{k}_{GC}^t(\mathbb{c} - \bar{c})}_{\text{transfer from gas channel}} + \underbrace{\bar{k}_{CO_2}^t(\bar{c}^B - \bar{c})}_{\text{transfer from electrolyte channel}} = \underbrace{\bar{k}\bar{c}}_{CO_2\text{ER reaction}} + \underbrace{\bar{c}_{OH^-}\bar{c}}_{\text{homogeneous reaction}},$$

(24)

$$\underbrace{\bar{k}_{H_2}^t(1 - \bar{c}_{OH^-})}_{\text{transfer from electrolyte channel}} + \underbrace{\bar{k}\bar{c}}_{CO_2\text{ER reaction}} + \underbrace{\bar{k}_{H_2}}_{H_2\text{ evolution}} = \underbrace{\bar{c}_{OH^-}\bar{c}}_{\text{homogeneous reaction}},$$

(25)

where $\bar{c}_{OH^-} \equiv \frac{C}{c_{OH^-}^B}$, $\bar{c}^B \equiv \frac{c_B}{c_0}$, $\bar{k}_{GC}^t \equiv \frac{k_{GC}^t}{L_{CL}\epsilon k_r c_{OH^-}^B}$, $\bar{k}_{CO_2}^t \equiv \frac{k_{CO_2}^t}{L_{CL}\epsilon k_r c_{OH^-}^B}$, $\bar{k}_{H_2}^t \equiv \frac{k_{OH^-}^t}{2L_{CL}\epsilon k_r c_0}$, $\bar{k} \equiv \frac{k}{k_r c_{OH^-}^B}$, and $\bar{k}_{H_2} \equiv \frac{k_{H_2}}{k_r c_0}$. Note the division by two in the definition of $\bar{k}_{H_2}^t$, as this will always be a two electron transfer reaction. It is worth noting that $\bar{k}_{CO_2}^t$ and $\bar{k}_{H_2}^t$ are determined by the development of the electrolyte flow channel, and may also be functions of $\bar{x}$ if required, as shown in (S39).

So far, we have refrained from including the effect of catalyst loading on $\bar{k}$ and $\bar{k}_{H_2}$. This is due to the fact that not all of the HER reaction necessarily takes place on catalyst particles, and some may instead take place on the CL substrate. Yang et al. showed that for catalyst deposited directly onto the GDL, a substantial portion, if not the majority, of HER takes place on the substrate [19]. However, they also showed that for a PTFE-based CL this effect is much less pronounced. HER on the

GDL does remain an issue in the case of electrolyte breakthrough and flooding.

We implement the effect of catalyst loading by taking $\bar{k} \to \theta\bar{k}$ for CO_2ER but $\bar{k}_{H_2} \to \frac{\theta+\theta_0}{1+\theta_0}\bar{k}$ for HER. Here θ_0 represents the ratio of substrate-based HER to total HER at full catalyst loading. A brief investigation of the impact of nonzero θ_0 is given in SI 3.3. Here we will assume that the PTFE content of our CL is sufficient to give $\theta_0 \approx 0$ and so rearrange (24) and (25) to

$$\bar{c} = \frac{\bar{k}_{GC}^t\bar{c} + \bar{k}_{CO_2}^t\bar{c}^B}{\bar{k}_{GC}^t + \bar{k}_{CO_2}^t + \theta\bar{k} + \bar{c}_{OH^-}},$$

(26)

$$\bar{c}_{OH^-} = \frac{\bar{k}_{H_2}^t + \theta\bar{k}\bar{c} + \theta\bar{k}_{H_2}}{\bar{k}_{H_2}^t + \bar{c}}.$$

(27)

Solving (26) and (27) for $\bar{c}$ and inserting that into (21), we arrive at

$$-\frac{\partial\bar{\mathbb{c}}}{\partial\bar{x}} = a\bar{c} + b - \sqrt{\alpha\bar{c}^2 + \beta\bar{c} + \gamma},$$

(28)

where the coefficients are given in (S47). This equation is solved numerically in MATLAB. Our addition of the additional flow channels requires a more nuanced performance metric, which we will consider now.

3.2. Performance metric

Although the reduction in total catalyst usage will save on electrolyser costs, we focus only on continuous operation efficiency. Factoring in catalyst values would necessitate bold assumptions about total cell material costs and lifespans, both of which are out of the scope of this work. We note that $n = 2$ corresponds to production of CO and consider the following,

ν_{CO_2},	the price of CO_2 in \$ mol^{-1},	(29a)
ν_{CO},	the price of CO in \$ mol^{-1},	(29b)
ν_P,	the price of electrical energy in \$ J^{-1}.	(29c)

We propose the following rough profit metric in units of \$ s^{-1} m^{-2}

$$Y_{\$} = \nu_{CO}Y^* - \nu_{CO_2}X^* - \nu_P(P_e + P_{sep}),$$

(30)

which includes the power input per unit area of electrode towards electrolysis P_e and separation P_{sep}, in J s^{-1} m^{-2}. The dimensional product yield and conversion per unit electrode area, Y^* and X^* respectively,

in mol s^{-1} m^{-2}:

$$Y^* = \frac{L_H L_{CL}}{A} \int_0^L \theta k c \, dx = X_{max}^* Y \frac{L_{CL}}{L_{GC}}, \qquad (31)$$

$$X^* = \frac{U L_H L_{GC}}{A} \left(c_0 - c(L) \right) = X_{max}^* X, \qquad (32)$$

where L_H is the cell height in the direction normal to the current and the flow and each quantity is normalised by cell area, $A = L_H L$. Here $X_{max}^* = \frac{U L_H L_{GC} c_0}{A} = \frac{U L_{GC} c_0}{L}$ is the maximum conversion per unit area. The faradaic efficiency S remains equal to that in (10), inserting $n = 2$. Note that in this $n = 2$ case, producing only CO and H_2, the total rate of electron charge transferred per unit area, C s^{-1} m^{-2}, or the average current density, can be written as

$$j = \frac{2F L_H L_{CL}}{A} \int_0^L \theta(kc + k_{H_2}) \, dx = \frac{2F L_{CL} c_0 k}{q} \int_0^1 \theta \left(q\bar{c} + 1 \right) d\bar{x} = 2F \frac{Y^*}{S}, \qquad (33)$$

where F is Faraday's constant. For a cell potential V, the power per unit area required for electrolysis is

$$P_e = jV = 2F \frac{Y^*}{S} V. \qquad (34)$$

Note that separation is currently routinely done through non-electrical means, but we assume future separation equipment will also be electrified. Although the produced H_2 has a value comparable to CO_2 per kg, the low molar mass of H_2 means the market value of the amount produced by HER is almost always negligible ($\approx 1\%$). We include the functionality in the MATLAB code and in the general case of the model, described in SI 2.5, but henceforth neglect H_2 in the profit metric. This general case also includes options for non-catalytic HER, electrolyte recombination and recirculation, crossover fractions, and user-defined liquid product separation costs. Often, besides the reactant CO_2 also other species are present at the gas channel inlet. However, for the sake of simplicity, we consider only reactants and products in our outlet gas stream. Therefore, we can approximately consider the energy cost of separation per mole of outlet gas, and then normalise the value by inlet flow rate to get a cost of separation per second. The minimum thermodynamic energy requirement of separation per second and unit area is thus given by

$$P_{sep}^* = -X_{sep}^* RT \sum_i x_i \ln x_i \qquad (35)$$

where $X_{sep}^* = \left(\frac{U L_H L_{GC}}{A} c_0 (1 - X) + \frac{j}{2F} \right) = X_{max}^* (1 - X) + \frac{Y^*}{S}$ is the total moles per second to be separated per unit electrode area. The first term represents the amount of CO_2 not converted, and the second term the amount of CO produced, both per second and per unit electrode area. Here x_i are the mole fractions in the outlet gas stream. Note that in SI 3.4, where we consider $n > 2$ for multiple product reduction, some fraction of the products may be liquid and thus remain in the liquid stream rather than the gas outlet, see SI 2.5. We dampen this ambitious minimum separation energy with an efficiency parameter μ through $P_{sep} = \frac{P_{sep}^*}{\mu}$ and note that for $n = 2$ reduction to CO and H_2

$$x_{CO_2} = \frac{X_{max}^* (1 - X)}{X_{sep}^*}, \qquad x_{CO} = \frac{Y^*}{X_{sep}^*}, \qquad x_{H_2} = \frac{Y^* - Y^* S}{S X_{sep}^*}. \qquad (36)$$

In addition, we consider the possibility of CO_2 crossover in the form of HCO_3^- and CO_3^{2-}. While often impeded by selective membranes, CO_2 crossover is difficult to fully prevent and leads to high recovery costs as it evolves into the anodic O_2 stream. Average costs are given by $v_A^* \approx 4$ MJ kg^{-1} [20,21]. We can determine the carbonate production rate by subtracting yield from conversion, and we can also introduce μ_c, the crossover efficiency, to describe the fraction of produced carbonates that cross over, react back to CO_2, and evolve at the anode. Using this

in (30), along with (34) and (35), gives a profit per second per unit area of

$$Y_\$ = v_{CO} Y^* - v_{CO_2} \left(X^* - \mu_c \left(X^* - Y^* \right) \right)$$
$$- v_P \left(2VF \frac{Y^*}{S} + v_A \mu_c \left(X^* - Y^* \right) - \frac{X_{sep}^* RT}{\mu} \sum_i x_i \ln x_i \right). \qquad (37)$$

By subtracting the crossed-over carbonate from X^* in the second term, we assume that from it the CO_2 will be fully recovered. However, we note that in the case of high anodic separation costs or low-cost reactant, it could occur that $v_{CO_2} < v_P v_A$, in which case it would be preferable to neglect the anodic separation step and simply pay for more reactant, as shown in SI. S2.

This metric is easily generalisable by replacing $v_{CO} Y^*$ with $v_i Y^i$ where i are each of the respective products, as is seen in SI. 3.4. We further note that the value of the produced H_2 is neglected from the analysis here for a fair comparison between reduction on Cu and Ag, as a likely output of an Ag-based electrolyser would actually be syngas rather than CO. An interested reader can enable the contribution of H_2 to the metric, as is shown in SI. 2.5, but herein we focus on CO alone, as a focus on syngas would lead to less clear conclusions due to varying outlet mole fraction price and as well as a neglection of H_2 separation cost.

3.3. Numerical method

In optimising the catalyst loading θ we will use (37) as the objective function. We will require as a constraint that the loading function, $\theta(\bar{x})$, must return a value on the interval $(0, 1]$, that is to say not including zero, must initially be unity, that is $\theta(0) = 1$, must be nonincreasing, that is $x > y \implies \theta(x) \leq \theta(y)$, integrates to some total catalyst loading value $\Theta = \int_0^1 \theta(\bar{x}) d\bar{x}$. For the sake of optimisation we will assume this function either takes a polynomial form,

$$\theta(\bar{x}) = \sum_{n=0}^N a_n \bar{x}^n, \qquad (38)$$

with coefficients a_n and $a_0 = 1$, or an equally spaced step function form with

$$\theta(\bar{x}) = \sum_{n=0}^N \left(a_n - a_{n-1} \right) H \left(\bar{x} - \frac{n}{N} \right), \qquad (39)$$

with $a_{-1} = 0$ and where $H(\bar{x})$ is the Heaviside function. This allows us to optimise for N coefficients describing the catalyst loading profile. We use a nonlinear optimiser in MATLAB with the above constraints to determine the optimal values of Θ and a_n by solving (28) numerically. Functional optimisation of (38) is simple due to the smoothness of polynomials, but the discontinuities presented by (39) necessitate stiff ODE solvers and spatial mesh refinement in the vicinity of steps, so we use *ode15s*. The resulting code can be freely downloaded as a supporting information file.

3.4. Results and discussion

3.4.1. Experimental comparison

While experimental works categorising the effects of undesired inhomogeneity in CL design exist [22], none to date selectively load the CL to balance mass transport and selectivity limitations. Nonetheless, Qi et al. [23] performed experiments with increasing numbers of layers of NPAu leaf catalyst. They found that at low current densities, where mass transport is unlikely to be an issue, the highest loading showed good selectivity, but at higher current densities, at which mass transport becomes more limited, the lower loading of 5 layers has the highest selectivity and lowest cell potential. This supports the claim that the excess catalyst present in the 10 layer case may be performing HER more than CO_2 electroreduction.

Table 1
Table of model parameters based on Kenis group flow electrolysers [25–28]. For a full description of the parameters, refer to S1, and table S1.

Symbol	Parameter	Value	Unit
L	Channel length	2×10^{-2}	m
L_H	Channel height	5×10^{-3}	m
L_{GC}	Gas channel width	2×10^{-3}	m
L_{EC}	Flow channel width	1.5×10^{-3}	m
L_{CL}	CL width	8×10^{-6}	m
X_{max}^*	Gas flow rate	17	ml min^{-1}
Q_L	Liquid flow rate	0.5	ml min^{-1}
ε	CL porosity	0.4	–
$\mathscr{H}$	CO_2 Henry constant	31.097	mol m^{-3} atm^{-1}
p_0	Initial pressure	1	atm
v_{CO_2}	Price of CO_2	3.1×10^{-3}	\$ mol^{-1}
v_{CO}	Price of CO	1.7×10^{-2}	\$ mol^{-1}
v_P	Price of electrical energy	1.4×10^{-8}	\$ J^{-1}
V	Cell potential	3	V
T	Temperature	293.15	K

Similarly, Löwe et al. found that for their high performance optimisation, the medium catalyst loadings performed best [24]. Excessive catalyst loadings led to high selectivity towards H_2, which we would predict is again due to excess catalyst being used for HER with insufficient CO_2 present due to mass transport limitations. Extremely low loadings, by contrast, simply struggled to attain sufficient current densities, due to a low effective exchange current density. Compared to 0.5 mg cm^{-2}, 5 mg cm^{-2} showed much better activity, but much higher stability and selectivity than 10 mg/cm^{-2}. Interestingly, at high current densities it also showed better selectivity than the 0.5 mg cm^{-2} case, giving credence to the claim that some substrates allow enough HER to have a significant effect on selectivity as the low-loading selectivity is also reported to be a function of the Nafion/PTFE ratio.

3.4.2. Reference gas flow rate

To date, there are no experimental studies on the effect of flow-wise catalyst loading variation in CO_2ER, so our comparison must be between the model with and without optimising catalyst loading. To accurately predict current densities from cell potentials would require additional closure relations in the forms of polarisation curves for each species and electrolyte current distributions. These are outside of the scope of this model, and seldom attain passable experimental matches, due in some degree to the difficulty in attaining exchange current densities as previously noted in the work of Sun et al. [18]. We instead aim to extract valid data from existing experimental setups and apply the optimisation using those derived kinetics. To determine geometric parameters, we take a generic microfluidic setup [26–28] and its operation conditions. In addition to the parameters in Table 1 we take the experimental total current density of $j = 477$ mA cm^{-2} with an FE of 91.2% at a gas flow rate of 17 ml min^{-1} in 3M KOH [28]. We then fit the reaction rate k and ratio q to the reported FE and current density and determine the maximum partial CO_2ER current density

$$j_{CO_2,0} = nFkc_0 L_{CL} \tag{40}$$

that would be obtained in case the concentration would be $c_0 = p_{CO_2}/RT$ through the whole CL. Using this fictitious, but non-arbitrary, high current density, we can write a reference value for flow rates as

$$Q_{ref} = \frac{j_{CO_2,0}A}{nFc_0}. \tag{41}$$

This maximum conversion of all inlet concentration c_0 is completely unattainable, so this flow rate should be seen more as an impartial reference flow rate. For the values in Table 1, $Q_{ref} \approx 24$ ml min^{-1}, and we note that this is in practice quite a high flow rate, so in Fig. 6 we consider flow rates of $Q = \frac{Q_{ref}}{2}$ and $Q = \frac{Q_{ref}}{4}$.

3.4.3. Optimised profiles for Ag

We see that, following (22), the aqueous concentration is far lower than the equilibrium concentration, due to the high electrochemical

and homogeneous reactions being at comparably high rates to the GDL mass transfer. By reducing the catalyst loading θ, the optimisation process decreases HER rate and thus pH in regions nearer to the outlet, permitting higher CO_2 concentrations. As the CO_2 electroreduction rate is first order in concentration, this increase mostly compensates for the reduction in catalyst availability. For example, in Fig. 6(b), $\bar{c}$ more than doubles and θ drops to a third of its initial value, meaning that the CO_2 electroreduction rate is reduced by less than a third while the HER is reduced by two thirds. Note that the optimised catalyst loading lowers the partial CO current density and also leads to a reduction in effectiveness metric $\mathcal{E} = YS$ of Fig. 2. However, the metric laid out in (37) is increased by roughly 0.6% and 4.5% in Fig. 6(a) and (b) respectively, as detailed in Section 3.4.5.

3.4.4. Optimised profiles for Cu

The efficacy of the optimisation is sensitive to reaction kinetics and gas flow rate, so we further investigate the optimisation process on a Cu catalyst cell, with reduction to multiple products with differing values of n. We replace these different reactions with one reaction with an effective n and k, in which different products are disambiguated by their respective experimentally fitted faradaic efficiencies. The value of n is then calculated as an average of electrons transferred for each product, weighted by each the respective faradaic efficiency of that product among CO_2ER products. A bold yet necessary assumption for the model is that reaction rates for each of the products remain first order in concentration. Using this assumption, we extract results from the work of Hoang et al. [29] kinetic parameters for the new system. They measured a total current density of 311 mA cm^{-2} and FE towards CO_2 products of 90.2% at a gas flow rate of 7 mL min. The observed products CO, HCOOH, CH_3OH, CH_4, C_2H_4, and C_2H_5OH on average used $n \approx 5$ electrons transferred per CO_2 converted. Notably, some of these products enter the liquid phase, but liquid separation is a less straightforward process to scale and is neglected from the metric. See SI 2.4 for more details. This lower current density and greater n combine to give a value of $Q_{ref} \approx 0.91$ mL min^{-1}, far lower than that of the Ag based cell. This is relevant, as Fig. 7 shows that the Cu based cell already reaches near full conversion of the gas supply at this reference flow rate in KOH, primarily due to the non-electrochemical conversion to carbonates, while the Ag cell does not reach full conversion at flow rates even as low as $\frac{Q_{ref}}{4}$.

A Cu catalyst based system encounters more issues with reactant utilisation than Ag in KOH as the high n means that the stoichiometric limit of (14) instead using $n \approx 5$ becomes

$$\lim_{q \to \infty} \bar{c} = e^{-\left(1 + \frac{5}{2}\right)Da \, \bar{x}} = e^{-3.5 Da \, \bar{x}}. \tag{42}$$

The relatively high average number of electrons transferred, n, used in (2) means there are more OH$^-$ ions to parasitically consume the CO_2. This manifests as an extremely high single pass conversion but low
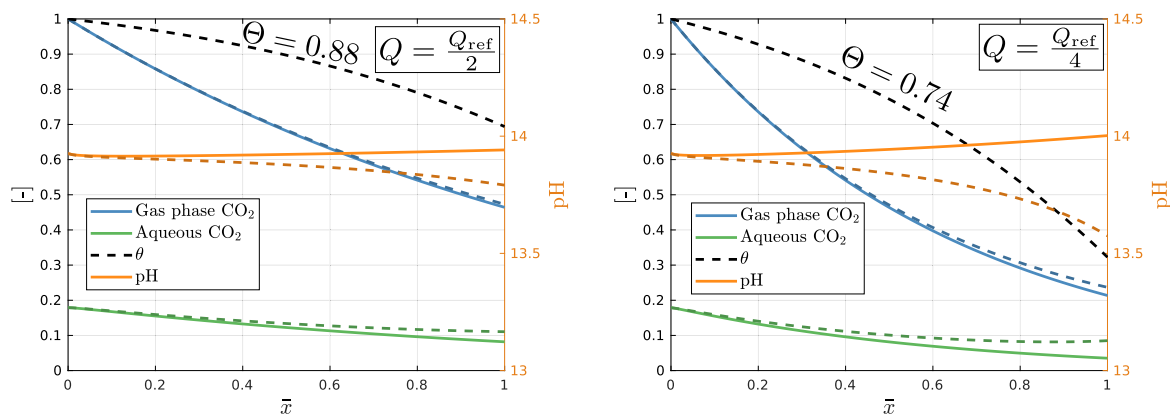
(a) Solutions to the numerical system for unoptimised (solid lines) and optimised (dashed lines) Ag catalyst loading, for a flow rate of $Q = \frac{Q_{ref}}{2}$, or approximately 12 mL min^{-1}.

(b) Solutions to the numerical system for unoptimised (solid lines) and optimised (dashed lines) Ag catalyst loading, for a flow rate of $Q = \frac{Q_{ref}}{4}$, or approximately 6 mL min^{-1}

Fig. 6. Solutions to the numerical system showing normalised gas phase concentration CO_2 ($\bar{c}$), aqueous phase concentration CO_2 ($\tilde{c}$), catalyst loading (θ), and pH, for reduction on an Ag catalyst in KOH. In Fig. 6(a), the single pass conversion is only slightly greater than 50% and a slight reduction of 12% in total catalyst loading increases selectivity from 90.4% to 91.3%, at the cost of reducing total current density from 436 mA cm^{-2} to 424 mA cm^{-2}. In Fig. 6(b), the single pass conversion now exceeds 70% and a large reduction of 26% in total catalyst loading roughly doubles the aqueous CO_2 concentration at the outlet and increases selectivity from 87.1% to 89.8%, at the cost of reducing total current density from 326 mA cm^{-2} to 303 mA cm^{-2}. In each case a reduced catalyst near the outlet improves selectivity at the cost of current density. The reduction in pH due to decreased HER current and the higher local aqueous CO_2 concentration combine to create a more favourable environment for electrochemical reaction of CO_2, despite a lower availability of catalyst in that region.
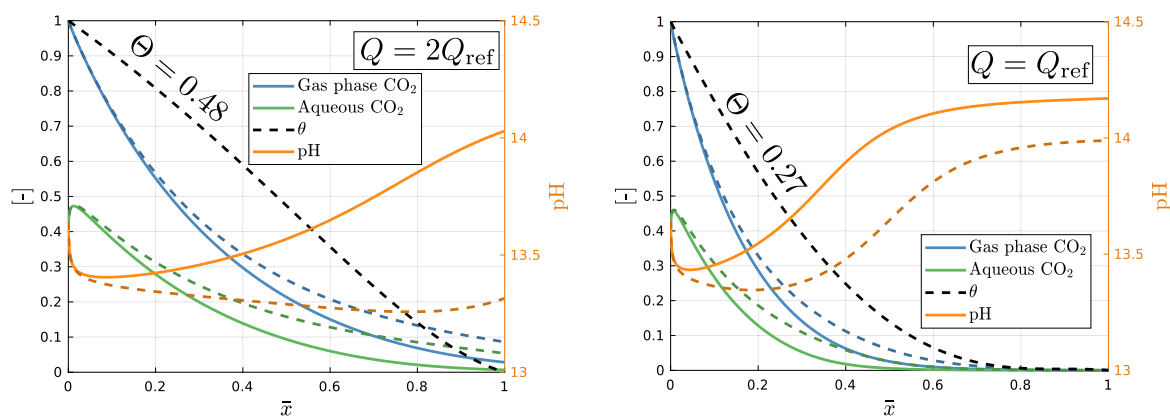
(a) Solutions to the numerical system for unoptimised (solid lines) and optimised (dashed lines) Cu catalyst loading at a flow rate of $Q = 2Q_{ref}$, or 1.82 mL min^{-1}.

(b) Solutions to the numerical system for unoptimised (solid lines) and optimised (dashed lines) Cu catalyst loading at a flow rate of $Q = Q_{ref}$, or 0.91 mL min^{-1}.

**Fig. 7.** Local plots of normalised gas phase CO_2 ($\bar{c}$), aqueous phase CO_2 ($\tilde{c}$), catalyst loading (θ), and pH for reduction on a Cu catalyst in KOH. In Fig. 7(a) the relatively low electrochemical reaction rate permits a higher aqueous CO_2 concentration near the inlet, but the high value of n means that this still constitutes a large OH$^-$ source. A reduction of 52% in catalyst loading greatly increases the selectivity from 78.8% to 87.4%, with a relatively small reduction in total current density from 141 mA cm^{-2} to 113 mA cm^{-2}. In Fig. 7(b) the effect of the high n and high pH of KOH are sufficient that all reactant is depleted early in the channel, despite Q_{ref} being ostensibly sufficient. The optimiser responds by completely removing catalyst in the depleted regions, fully eliminating the unnecessary HER and greatly improving selectivity from 63.9% to 85.3% with a reduction in total current density from 82 mA cm^{-2} to 55 mA cm^{-2}. High OH$^-$ production from the CO_2 reduction as well as HER means that the local pH increases to extreme levels in the unoptimised system, even exceeding the high KOH pH in the latter regions. It becomes preferable for the optimiser to remove large amounts of catalyst to reduce electricity cost from HER, as it is practically impossible for the electrochemical reaction rate to compete with the homogeneous reaction rate and yield more product.

yield, motivating the optimiser to drastically decrease θ in the reactant depleted regions. We can track CO_2 in the model to find that in Fig. 6 roughly 45% of the reactant that enters the CL is converted to CO, but in each case in Fig. 7 only around 15% is converted to products. This means that of the almost unity single pass conversion, around 80% is simply converted to carbonates, representing a large cost in reactant loss and anodic separation.

3.4.5. Cost breakdown for Ag

The relevant costs for the Ag and Cu cases discussed above are shown in Figs. 9(a) and (b), respectively. From Fig. 9(a) we see the change in cost distribution after optimisation is subtle. Despite significant catalyst removal, the distribution and the total costs only slightly

change. The majority of the cost comes from electrolysis energy, with reactant and anodic separation costs playing a smaller yet significant role. It is noted that this anodic separation step is to recover CO_2 that has crossed over, so can be viewed as an additional reactant cost. Furthermore, as this process depends on the price of electricity v_P rather than the price of CO_2, v_{CO_2}, so we must be careful to ensure that the step remains feasible. In fact, if v_{CO_2} were to drop by roughly 20%, it would be cheaper to simply purchase more CO_2 rather than waste electricity recovering it from the anode stream. To some extent, this anodic separation cost can be seen as an energy cost due to poor reactant utilisation rather than a direct reactant cost. Improvements in profit margins are 0.6% and 4.5% respectively after optimisation for the used lower and higher flow rates. To these modest improvements a small saving in catalyst costs can be added.
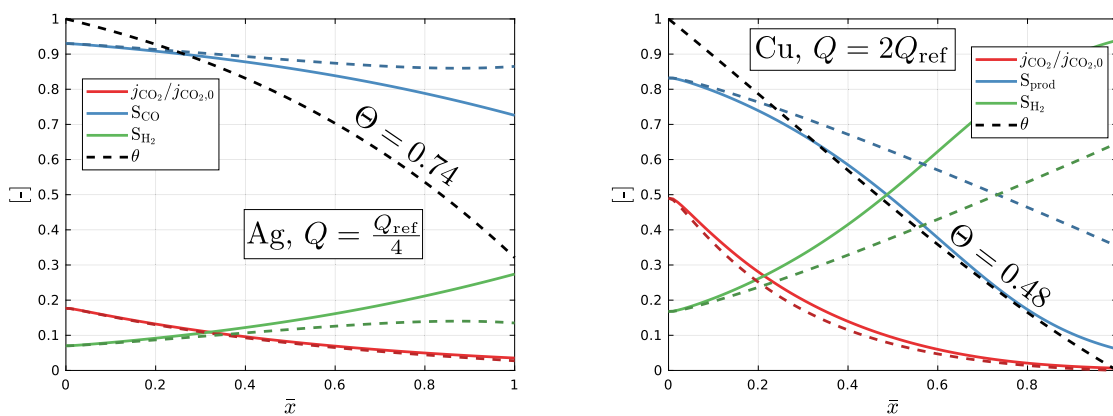
(a) Normalised partial CO_2 current densities and product and H_2 selectivities before and after optimisation for the case of reduction on Ag depicted in Fig. 6a

(b) Normalised partial CO_2 current densities and product and H_2 selectivities before and after optimisation for the case of reduction on Cu depicted in Fig. 7a

Fig. 8. Profiles after optimisation, denoted by dashed lines, show that the selectivity towards CO_2 reduction products is significantly increased, the selectivity towards H_2 is significantly reduced, and the normalised current density is relatively unchanged. The effects are far more pronounced in Fig. 8(b), in which the gradient of θ is far steeper and the average number of electrons transferred, n, is much higher.
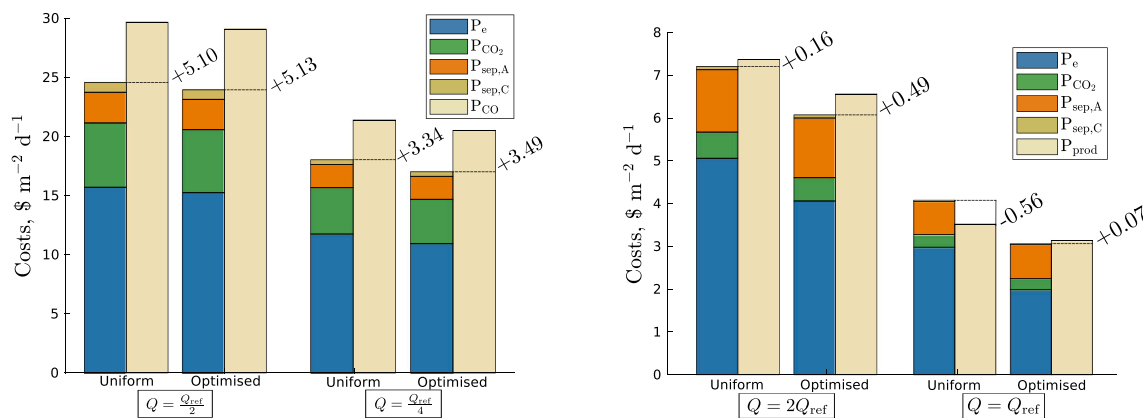
(a) Breakdown of the costs associated with electrolyser operation and value of produced CO for reduction on Ag in KOH for the systems in Fig. 6. The net profits are labeled above the dashed lines.

(b) Breakdown of the costs associated with electrolyser operation and value of produced CO for reduction on Cu in KOH for the systems in Fig. 7. The net profits, or in the third case, losses, are labeled above the dashed lines.

Fig. 9. Bars representing the costs of electricity, P_e, reactant, P_{CO_2}, anodic separation, $P_{sep,A}$, cathodic separation, $P_{sep,C}$ and product chemicals, and the revenues P_{CO} and P_{prod} are shown for each system, in units of dollars per square metre of electrolyser area per day. The net profits are labelled above the dashed lines. In every case, electricity costs dominate, and profit margin is improved by decreasing costs while attempting to maintain high product yield.

3.4.6. Cost breakdown for Cu

Fig. 9(b) shows a more tempered picture of reduction on Cu. Despite higher normalised flow rates, the profit margins are much smaller (note the different y-axis scaling), and even negative in the unoptimised case using Q_{ref}. Due to the higher value of n, the fraction of cost from converted CO_2 is far smaller and electrolysis energy cost remains dominant. The lower profit is clearly not due to a decrease in conversion, as Fig. 7 shows near unity conversion, but is actually due to a low portion of CO_2 being converted to products. The high anodic separation costs represent the overwhelming fraction of CO_2 being converted to carbonates and crossing over. Notably, the cathodic separation costs are small, for a number of reasons: low outlet CO_2 concentrations, due to high single pass conversion; decreased product concentrations for non-CO products, due to higher n values yielding fewer moles of products; and the fact that for reduction on Cu a significant portion of products remain in the liquid phase, so they have no impact on the cathodic gas stream separation cost. The improvements due optimising the catalyst loading in this case are large, from a tripling in profit margin in the higher flow rate case to a recovery from severe loss to minor profit in the lower flow rate case.

3.5. Discussion

Across all of Fig. 9, we see that a system with a lower gas flow rate is more strongly optimised with a lower value of Θ and a larger improvement in profit margin. However, we also see that simply a higher flow rate leads to a greater profit margin, despite the increase in reactant cost, increase in separation cost, and decrease in single pass conversion. Despite being a serious, even titular, focus in literature studies, single-pass conversion is not always a good metric for CO_2 electroreduction performance. In concurrence with more recent techno-economic analyses, we find that anodic separation costs dominate cathodic separation costs [21], but more importantly, electrolyser energy dominates both [30]. Moore et al. neatly show that the energy optima frequently lie at low single pass conversions of less than 10%, and we can similarly show our agreement with this conclusion by manipulating flow rate rather than current density to attain various single pass conversions. Fig. 10 shows that indeed, low single pass conversions, achieved by high flow rates, exhibit the highest profit margins, and the largest cost is always P_e by a significant margin.

When additional products are considered the number of electrons transferred is vital, as noted in Eq. (42). In Fig. 11 the primary product
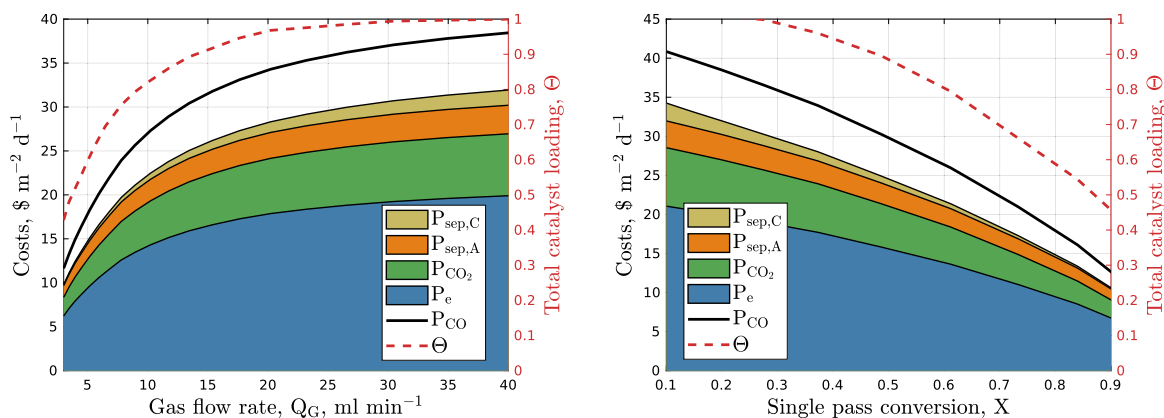
(a) Stacked costs, optimised Θ, and product value for optimised reduction in KOH on Ag for the kinetics in Table 1 at varying flow rate, X^*_{max}. Low X^*_{max} necessitates low Θ to manage reactant limitations, whereas high X^*_{max} systems require little to no optimisation for these parameters.

(b) Stacked costs, optimised Θ, and product value for optimised reduction in KOH on Ag for the kinetics in Table 1 at varying single pass conversions, X. High single pass conversions require low Θ, but single pass conversions lower than 0.25 are optimised by maximising Θ.

Fig. 10. Low flow rates correspond to high single pass conversions and low optimised Θ, to alleviate reactant shortages, whereas high flow rates yield low single pass conversions, higher optimal Θ, and, in agreement with Moore et al. higher profit margins. At low single pass conversions, or equivalently very high gas flow rates, Θ reaches unity, meaning that the reactant supply is high enough that the electrolyser is operating effectively along its entire length.

is continuously varied from 55% FE towards C_2H_4 to 55% FE towards HCOOH, with n values of 6 and 2 respectively. It shows that HCOOH is preferable not only due to its higher value per transferred electron, but also leads to a lower anodic separation cost, $P_{sep,A}$ as less electrochemically produced OH^- is available to convert CO_2 to carbonates. This increased ratio between P_{CO_2} and $P_{sep,A}$ is also indicative of a higher CO_2 utilisation, allowing higher single pass conversions to remain feasible and thus optimal values of Θ to be higher.

A recommendation following from this information is to simply make the electrolyser shorter or to increase gas flow rate, both of which have a similar positive effect. Indeed, this is the conclusion found for the simple model in Section 2. However, from a practical and economical perspective longer electrolysers may be preferred and there are also limitations to the maximum gas flow rate that can be used. High flow rates lead to turbulence and high pressure drops that can lead to pressure-balancing problems that can cause catalyst drying or electrode flooding. Therefore, often sub-optimal flow rates are used in practice for which a variable catalyst loading can generate significant benefits as shown in this work. In some systems that exhibit $\Theta < 1$ even at extremely low single pass conversions, the optimisation process can be degenerate. This can correspond to systems that are limited by insufficient mass transfer through the GDL or systems that are always economically infeasible. In the former case, Θ becomes independent of flow rate and instead depends on GDL mass transfer rate. This change can be reverted by simply lowering the current density, similar to the conclusion of the 1D model, or by improving mass transfer through the GDL or increasing c_0 by increasing $p_{CO_2,0}$.

3.5.1. Limitations and extensions

The model presented here is generalisable to a wide range of systems, but there are some boundaries to what is achievable. Firstly, it is important to consider that the reaction order of CO_2 at the catalyst may vary for different catalysts and reduction products. Different rate-limiting steps lead to different order dependencies on CO_2 concentration, pH, and even HCO_3^- as a reactant in neutral pH [31]. The model assumes first order dependence in CO_2 concentration for electroreduction, but similar equations can be derived for second order or even fractional dependence on CO_2 concentration. However, if multiple products have different order dependencies, as is possible for a Cu catalyst producing C_1 and C_{2+} products simultaneously, then Eq. (22) and (23) would require additional terms and it would become more expedient to solve the entire system numerically. This is generally the

case across all different catalysts and products, and is merely a limitation to the model used in this work, not to variable catalyst loading in general. Another consideration is that the range of dimensionless loadings, $\theta \in (0, 1]$, must roughly lie within the range where increased loading does not significantly affect the structure of the CL.

Furthermore, the assumption required for Eq. (8) is that the pH is sufficiently high that the carbonate buffer reaction can be collapsed into a single $2OH^-$ reaction, and this theoretically precludes the use of the model with neutral or acidic electrolytes. However, Bernasconi et al. showed that even in strongly acidic (pH 1) electrolytes, the local environment at the CL can still become so alkaline at high current densities that carbonate precipitation still becomes an issue [32]. As this assumption in Eq. (8) only actually requires a high pH within the CL, it will thus be true when operating at sufficient current density, regardless of the choice of electrolyte. At lower current densities however, both assumptions in Eq. (8) of single step buffering and of zeroth order HER will break down, as the low pH will lead to the majority of HER being first order in H^+ concentration, as well as additional contribution of direct reduction from HCO_3^- [33]. It is thus recommended to only use the provided model at high current densities when considering acidic or neutral media. Nonetheless, reduction in acidic media usually comes at the cost of high HER due to H^+ abundance, and aims to achieve high single-pass conversion due to reduced buffer reactions, both of which could lead to the outlet regions having poor FE. As electrolysis, and by extension FE, is the predominant cost even when crossover is severe, we predict that variable catalyst will be similarly useful in electrolysers implementing acidic electrolytes.

3.5.2. Future prospects

We have shown that variable catalyst loading can yield solid results in lab-scale electrolysers, but we also show that systems that already operate efficiently are likely to gain little benefit from it. In many cases, simply using a shorter electrolyser, higher gas flow rate, or lower current density, is sufficient to circumvent these issues without the need for selective loading. Nonetheless, it is important to reiterate that this proposed method of selective catalyst loading lacks a significant opportunity cost: even if a small or negligible effect on performance is achieved, the capital cost of catalyst is reduced. While this might only consist of a small saving for Sn and Ni based electrodes, highly selective future cathodes could depend on expensive Cu-based metallic organic frameworks and extremely expensive anodic Ir catalysts [34], for which the reduction in capital cost from variable catalyst loading would be considerable.
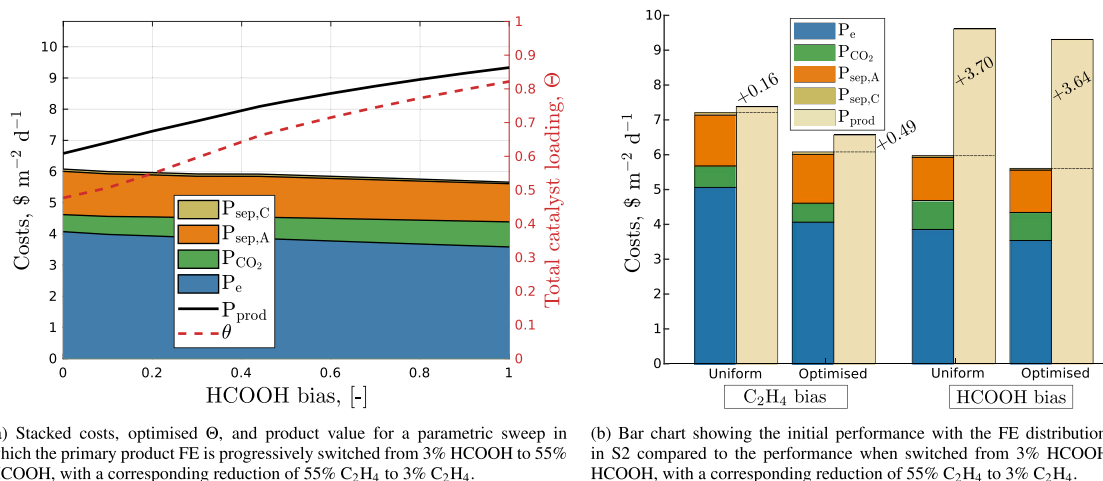

(a) Stacked costs, optimised Θ, and product value for a parametric sweep in which the primary product FE is progressively switched from 3% HCOOH to 55% HCOOH, with a corresponding reduction of 55% C₂H₄ to 3% C₂H₄.

(b) Bar chart showing the initial performance with the FE distribution detailed in S2 compared to the performance when switched from 3% HCOOH to 55% HCOOH, with a corresponding reduction of 55% C₂H₄ to 3% C₂H₄.

Fig. 11. Plots comparing a selectivity bias towards C_2H_4, as seen in the reduction on a Cu catalyst in the setup of Fig. 7(a), with an equivalent setup with a biased selectivity towards HCOOH. The initial selectivities seen in Table S2, are scaled from 3% FE to 55% FE towards HCOOH, and the opposite for C_2H_4, while maintaining the same first order reaction rate. While the large increase in revenue can be attributed to the greater value of HCOOH per mole, it is also worth noting that P_{CO_2} significantly increases and $P_{sep,A}$ decreases, as a much greater portion of reactant CO_2 is converted to product than carbonates. This is due to the much lower value of $n = 2$ for HCOOH, compared to $n = 6$ for C_2H_4, which means two-thirds less OH^- is electrochemically produced per reduced CO_2, and much less CO_2 is buffered away into carbonates. The low n value also means that for the same initial current density more CO_2 is reduced per transferred electron, and along with the high price of HCOOH a high Θ and high single pass conversion are possible.

The ideal form of CO_2 reduction would be the direct reduction of flue gas, due to its abundance and low cost, but the high O_2 content would necessitate high current densities to overcome the competitive O_2 reduction reaction [35], and combined with the relatively low CO_2 content this would likely lead to the same high single-pass conversions for which variable catalyst loading showed the greatest improvement. Also, considering that lab-scale electrolysers often struggle with long-term stability, it is likely that industrial scale electrolyser will have to make significant concessions to ensure that salt precipitation, electrolyte breakthrough, and flooding are mitigated. These phenomena are often correlated, as a high local pH leads to carbonate supersaturation, precipitation, and subsequent substrate damage, causing loss of hydrophobicity, crack formation, and eventually differential pressure imbalance and flooding [36]. Variable catalyst loading can both mitigate the effects of suboptimal flow rates necessary to balance pressure drops between the flow channels, and can aid in reducing the local CL pH to prevent salt precipitation.

Another note is that the concentration boundary layer in an industrial flow electrolyser could be broken up by periodic static mixers, increasing the influence of the electrolyte boundary transfer terms in Eqs. (22) and (23). The impact this would have on variable catalyst loading depends on the choice of electrolyte and current density, as it would be beneficial in reducing CL pH with neutral or acidic pH, but would actually serve to increase CL pH in low-to-medium current densities in alkaline media, while also permitting higher carbonate crossover. As improved flow architectures, such as serpentine or interdigitated flow channels, are simulated to locate and minimise reaction dead-zones, the impact of variable catalyst loading will decrease [37]. However, simulations showing the location and intensity of reaction dead-zones can show exactly the regions and regimes in which a selective reduction in catalyst loading would be useful, and can ideally work together to further improve catalyst utilisation.

4. Conclusion

We considered first-order reaction systems with competitive secondary reactions, showing how these can be optimised with selective reduction in catalyst. We first derived an analytical solution for simple 1D electrochemical flow cells, in which secondary reactions produce reactant annihilating species. Using analytical solutions for different catalyst loading profiles we show that improvements are possible at higher Damköhler numbers, corresponding to lower gas flow rates or longer channels. Variable catalyst loading yields greater results in systems with prevalent buffer reactions.

We further the investigation by developing a model of a GDE based CO_2 electrolyser, with a more comprehensive cost metric to consider more realistic operation. In doing so, we find that many typical electrolyser setups can benefit from carefully engineered catalyst distribution, and while some systems may not receive a large benefit it must be reiterated that this benefit is effected by, in fact, a *reduction* in catalyst capital cost. This means that this optimisation should always be considered. Furthermore, we find agreement with recent literature that a singular focus on single pass conversion or reactant utilisation may be misguided, as electrolyser energy is the predominant cost in such cells, and peak performance is reached at low single pass conversions. We further find that, while variable catalyst loading has the greatest impact on high single pass conversion systems, there are parameter spaces in which variable catalyst loading will have a large impact regardless of single pass conversion. As such, we recommend that interested readers use and adapt the provided MATLAB code to investigate the potential benefits of this optimisation process in their own systems.

CRediT authorship contribution statement

J.W. Blake: Conceptualization, Formal analysis, Methodology, Software, Writing – original draft. **J.W. Haverkort:** Conceptualization, Formal analysis, Funding acquisition, Methodology, Validation, Writing – review & editing. **J.T. Padding:** Conceptualization, Methodology, Supervision, Writing – review & editing.

Declaration of competing interest

The authors declare that they have no known competing financial interests or personal relationships that could have appeared to influence the work reported in this paper.

Data availability

The MATLAB files have been made freely available in the supplementary information.

Acknowledgements

Appendix A. Supplementary data

Supplementary material related to this article can be found online at https://doi.org/10.1016/j.electacta.2024.145177.

References

[1] T. Burdyny, W.A. Smith, CO_2 reduction on gas-diffusion electrodes and why catalytic performance must be assessed at commercially-relevant conditions, Energy Environ. Sci. 12 (2019) 1442–1453, http://dx.doi.org/10.1039/C8EE03134G.

[2] Y. Li, N.M. Adli, W. Shan, M. Wang, M.J. Zachman, S. Hwang, H. Tabassum, S. Karakalos, Z. Feng, G. Wang, Y.C. Li, G. Wu, Atomically dispersed single Ni site catalysts for high-efficiency CO_2 electroreduction at industrial-level current densities, Energy Environ. Sci. 15 (2022) 2108–2119, http://dx.doi.org/10.1039/D2EE00318J.

[3] M. Sassenburg, R. de Rooij, N.T. Nesbitt, R. Kas, S. Chandrashekar, N.J. Firet, K. Yang, K. Liu, M.A. Blommaert, M. Kolen, D. Ripepi, W.A. Smith, T. Burdyny, Characterizing CO_2 reduction catalysts on gas diffusion electrodes: Comparing activity, selectivity, and stability of transition metal catalysts, ACS Appl. Energy Mater. 5 (5) (2022) 5983–5994, http://dx.doi.org/10.1021/acsaem.2c00160.

[4] G.O. Larrazábal, M. Ma, B. Seger, A comprehensive approach to investigate CO_2 reduction electrocatalysts at high current densities, Accounts Mater. Res. 2 (4) (2021) 220–229, http://dx.doi.org/10.1021/accountsmr.1c00004.

[5] D. Tian, Z. Qu, J. Zhang, Electrochemical condition optimization and techno-economic analysis on the direct CO_2 electroreduction of flue gas, Appl. Energy 351 (2023) 121787, http://dx.doi.org/10.1016/j.apenergy.2023.121787, URL: https://www.sciencedirect.com/science/article/pii/S0306261923011510.

[6] Y. Cheng, P. Hou, X. Wang, P. Kang, CO_2 electrolysis system under industrially relevant conditions, Acc. Chem. Res. 55 (3) (2022) 231–240, http://dx.doi.org/10.1021/acs.accounts.1c00614, PMID: 35045254.

[7] P. Jeanty, C. Scherer, E. Magori, K. Wiesner-Fleischer, O. Hinrichsen, M. Fleischer, Upscaling and continuous operation of electrochemical CO_2 to CO conversion in aqueous solutions on silver gas diffusion electrodes, J. CO_2 Util. 24 (2018) 454–462, http://dx.doi.org/10.1016/j.jcou.2018.01.011, URL: https://www.sciencedirect.com/science/article/pii/S2212982017307084.

[8] J.W. Blake, V. Konderla, L.M. Baumgartner, D.A. Vermaas, J.T. Padding, J.W. Haverkort, Inhomogeneities in the catholyte channel limit the upscaling of CO_2 flow electrolysers, ACS Sustain. Chem. Eng. 11 (7) (2023) 2840–2852, http://dx.doi.org/10.1021/acssuschemeng.2c06129.

[9] M. Goldman, A. Prajapati, E. Duoss, S. Baker, C. Hahn, Bridging fundamental science and applied science to accelerate CO_2 electrolyzer scale-up, Curr. Opin. Electrochem. 39 (2023) 101248, http://dx.doi.org/10.1016/j.coelec.2023.101248, URL: https://www.sciencedirect.com/science/article/pii/S2451910323000418.

[10] A. Somoza-Tornos, O.J. Guerra, A.M. Crow, W.A. Smith, B.-M. Hodge, Process modeling, techno-economic assessment, and life cycle assessment of the electrochemical reduction of CO_2: A review, iScience 24 (7) (2021) http://dx.doi.org/10.1016/j.isci.2021.102813.

[11] H. Simonson, W.E. Klein, D. Henckel, S. Verma, K.C. Neyerlin, W.A. Smith, Direct measurement of electrochemical selectivity gradients over a 25 cm^2 copper gas diffusion electrode, ACS Energy Lett. 8 (9) (2023) 3811–3819, http://dx.doi.org/10.1021/acsenergylett.3c01489.

[12] R. Kas, A.G. Star, K. Yang, T. Van Cleve, K.C. Neyerlin, W.A. Smith, Along the channel gradients impact on the spatioactivity of gas diffusion electrodes at high conversions during CO_2 electroreduction, ACS Sustain. Chem. Eng. 9 (3) (2021) 1286–1296, http://dx.doi.org/10.1021/acssuschemeng.0c07694.

[13] A. Kulikovsky, A model for optimal catalyst layer in a fuel cell, Electrochim. Acta 79 (2012) 31–36, http://dx.doi.org/10.1016/j.electacta.2012.06.069, URL: https://www.sciencedirect.com/science/article/pii/S0013468612010456.

[14] A. Kulikovsky, Optimal shape of catalyst loading across the active layer of a fuel cell, Electrochem. Commun. 11 (10) (2009) 1951–1955, http://dx.doi.org/10.1016/j.elecom.2009.08.026, URL: https://www.sciencedirect.com/science/article/pii/S138824810900397X.

[15] A. Kulikovsky, Optimal shape of catalyst loading along the oxygen channel of a PEM fuel cell, Electrochim. Acta 54 (27) (2009) 7001–7005, http://dx.doi.org/10.1016/j.electacta.2009.07.005, URL: https://www.sciencedirect.com/science/article/pii/S0013468609009438.

[16] T. Moore, T.Y. Lin, T. Roy, S.E. Baker, E.B. Duoss, C. Hahn, V.A. Beck, Simplified models of the bicarbonate buffer for scaled simulations of CO_2 electrolyzers, Ind. Eng. Chem. Res. 62 (40) (2023) 16291–16301, http://dx.doi.org/10.1021/acs.iecr.3c02504.

[17] J.W. Haverkort, Electrolysers, Fuel Cells and Batteries: Analytical modelling, TU Delft Open Publishing, 2024.

[18] Y. Sun, J. Lu, L. Zhuang, Rational determination of exchange current density for hydrogen electrode reactions at carbon-supported Pt catalysts, Electrochim. Acta 55 (3) (2010) 844–850, http://dx.doi.org/10.1016/j.electacta.2009.09.047, URL: https://www.sciencedirect.com/science/article/pii/S0013468609012067.

[19] K. Yang, R. Kas, W.A. Smith, T. Burdyny, Role of the carbon-based gas diffusion layer on flooding in a gas diffusion electrode cell for electrochemical CO_2 reduction, ACS Energy Lett. 6 (1) (2021) 33–40, http://dx.doi.org/10.1021/acsenergylett.0c02184.

[20] T. Alerte, J.P. Edwards, C.M. Gabardo, C.P. O'Brien, A. Gaona, J. Wicks, A. Obradović, A. Sarkar, S.A. Jaffer, H.L. MacLean, D. Sinton, E.H. Sargent, Downstream of the CO_2 electrolyzer: Assessing the energy intensity of product separation, ACS Energy Lett. 6 (12) (2021) 4405–4412, http://dx.doi.org/10.1021/acsenergylett.1c02263.

[21] K. Xie, A. Ozden, R.K. Miao, Y. Li, D. Sinton, E.H. Sargent, Eliminating the need for anodic gas separation in CO_2 electroreduction systems via liquid-to-liquid anodic upgrading, Nature Commun. 13 (1) (2022) 3070, http://dx.doi.org/10.1038/s41467-022-30677-x.

[22] G. Liu, D. McLaughlin, S. Thiele, C. Van Pham, Correlating catalyst ink design and catalyst layer fabrication with electrochemical CO2 reduction performance, Chem. Eng. J. 460 (2023) 141757, http://dx.doi.org/10.1016/j.cej.2023.141757, URL: https://www.sciencedirect.com/science/article/pii/S1385894723004886.

[23] Z. Qi, M.M. Biener, A.R. Kashi, S. Hunegnaw, A. Leung, S. Ma, Z. Huo, K.P. Kuhl, J. Biener, Electrochemical CO_2 to CO reduction at high current densities using a nanoporous gold catalyst, Mater. Res. Lett. 9 (2) (2021) 99–104, http://dx.doi.org/10.1080/21663831.2020.1842534.

[24] A. Löwe, M. Schmidt, F. Bienen, D. Kopljar, N. Wagner, E. Klemm, Optimizing reaction conditions and gas diffusion electrodes applied in the CO_2 reduction reaction to formate to reach current densities up to 1.8 a cm^{-2}, ACS Sustain. Chem. Eng. 9 (11) (2021) 4213–4223, http://dx.doi.org/10.1021/acssuschemeng.1c00199.

[25] D.T. Whipple, E.C. Finke, P.J.A. Kenis, Microfluidic reactor for the electrochemical reduction of carbon dioxide: The effect of pH, Electrochem. Solid-State Lett. 13 (9) (2010) B109, http://dx.doi.org/10.1149/1.3456590.

[26] B. Kim, S. Ma, H.-R. Molly Jhong, P.J. Kenis, Influence of dilute feed and pH on electrochemical reduction of CO_2 to CO on Ag in a continuous flow electrolyzer, Electrochim. Acta 166 (2015) 271–276, http://dx.doi.org/10.1016/j.electacta.2015.03.064, URL: http://www.sciencedirect.com/science/article/pii/S0013468615006465.

[27] S. Ma, R. Luo, S. Moniri, Y. Lan, P.J.A. Kenis, Efficient electrochemical flow system with improved anode for the conversion of CO_2 to CO, J. Electrochem. Soc. 161 (10) (2014) F1124, http://dx.doi.org/10.1149/2.1201410jes.

[28] S. Verma, X. Lu, S. Ma, R.I. Masel, P.J.A. Kenis, The effect of electrolyte composition on the electroreduction of CO_2 to CO on Ag based gas diffusion electrodes, Phys. Chem. Chem. Phys. 18 (2016) 7075–7084, http://dx.doi.org/10.1039/C5CP05665A.

[29] T.T.H. Hoang, S. Verma, S. Ma, T.T. Fister, J. Timoshenko, A.I. Frenkel, P.J.A. Kenis, A.A. Gewirth, Nanoporous copper–silver alloys by additive-controlled electrodeposition for the selective electroreduction of CO_2 to ethylene and ethanol, J. Am. Chem. Soc. 140 (17) (2018) 5791–5797, http://dx.doi.org/10.1021/jacs.8b01868, PMID: 29620896.

[30] T. Moore, D.I. Oyarzun, W. Li, T.Y. Lin, M. Goldman, A.A. Wong, S.A. Jaffer, A. Sarkar, S.E. Baker, E.B. Duoss, C. Hahn, Electrolyzer energy dominates separation costs in state-of-the-art CO_2 electrolyzers: Implications for single-pass CO_2 utilization, Joule 7 (4) (2023) 782–796, http://dx.doi.org/10.1016/j.joule.2023.03.015, URL: https://www.sciencedirect.com/science/article/pii/S2542435123001277.

[31] M. Dunwell, W. Luc, Y. Yan, F. Jiao, B. Xu, Understanding surface-mediated electrochemical reactions: CO_2 reduction and beyond, ACS Catal. 8 (9) (2018) 8121–8129, http://dx.doi.org/10.1021/acscatal.8b02181.

[32] F. Bernasconi, N. Plainpan, M. Mirolo, Q. Wang, P. Zeng, C. Battaglia, A. Senocrate, Operando observation of (Bi)carbonate precipitation during electrochemical CO_2 reduction in strongly acidic electrolytes, ACS Catal. (2024) 8232–8237, http://dx.doi.org/10.1021/acscatal.4c01884.

[33] E.W. Lees, M. Goldman, A.G. Fink, D.J. Dvorak, D.A. Salvatore, Z. Zhang, N.W.X. Loo, C.P. Berlinguette, Electrodes designed for converting bicarbonate into CO, ACS Energy Lett. 5 (7) (2020) 2165–2173, http://dx.doi.org/10.1021/acsenergylett.0c00898.

[34] C. Minke, M. Suermann, B. Bensmann, R. Hanke-Rauschenbach, Is iridium demand a potential bottleneck in the realization of large-scale PEM water electrolysis? Int. J. Hydrog. Energy 46 (46) (2021) 23581–23590, http://dx.

doi.org/10.1016/j.ijhydene.2021.04.174, URL: https://www.sciencedirect.com/science/article/pii/S0360319921016219.

[35] S. Van Daele, L. Hintjens, S. Hoekx, B. Bohlen, S. Neukermans, N. Daems, J. Hereijgers, T. Breugelmans, How flue gas impurities affect the electrochemical reduction of CO_2 to CO and formate, Appl. Catal. B 341 (2024) 123345, http://dx.doi.org/10.1016/j.apcatb.2023.123345, URL: https://www.sciencedirect.com/science/article/pii/S0926337323009888.

[36] E.R. Cofell, U.O. Nwabara, S.S. Bhargava, D.E. Henckel, P.J.A. Kenis, Investigation of electrolyte-dependent carbonate formation on gas diffusion electrodes for CO_2 electrolysis, ACS Appl. Mater. Interfaces 13 (13) (2021) 15132–15142, http://dx.doi.org/10.1021/acsami.0c21997, PMID: 33764731.

[37] M. Filippi, T. Möller, L. Liang, P. Strasser, Understanding the impact of catholyte flow compartment design on the efficiency of CO_2 electrolyzers, Energy Environ. Sci. 16 (2023) 5265–5273, http://dx.doi.org/10.1039/D3EE02243A.